PERGAMON

www.elsevier.nl/locate/poly

Polyhedron 19 (2000) 655–664

POLYHEDRON

Electrochemical and X-ray studies of nickel(II) Schiff base complexes derived from salicylaldehyde. Structural effects of bridge substituents on the stabilisation of the +3 oxidation state

I.C. Santos [a], M. Vilas-Boas [a], M.F.M. Piedade [c,d], C. Freire [a,*], M.T. Duarte [b,d], B. de Castro [a]

[a] *CEQUP/Departamento de Química, Faculdade de Ciências, Universidade do Porto, Rua do Campo Alegre 687, P-4169-007 Porto, Portugal*

[b] *Instituto Superior Técnico, Universidade Técnica de Lisboa, Lisbon, Portugal*

[c] *Departamento de Química e Bioquímica, Faculdade de Ciências, Universidade de Lisboa, Lisbon, Portugal*

[d] *Centro de Química Estrutural, I.S.T, Lisbon, Portugal*

Received 10 August 1999; accepted 13 January 2000

Abstract

The oxidative chemistry of three Ni(II) complexes with Schiff base ligands derived from salicylaldehyde and diamines with different steric demands, *N*,*N*′-2-methylpropane-2,3-diyl-bis(salicylideneiminate)nickel(II) (**1**), *N*,*N*′-1,2-cyclohexyl-1,2-dyil-bis(salicylideneiminate)-nickel(II) (**2**) and *N*,*N*′-2,3-dimethylbutane-2,3-diyl-bis(salicylideneiminate)nickel(II) (**3**), was studied by cyclic voltammetry and chronoamperometry in *N*,*N*′-dimethylformamide and $(CH_3)_2SO$. The electrogenerated species were characterised by EPR spectroscopy. All three complexes exhibited metal-centred oxidised processes and the oxidised products were low-spin six-coordinate Ni(III) species (d_{z^2} ground state) with two solvent molecules axially coordinate. Addition of pyridine resulted in the replacement of solvent molecules with no changes in the ground state. The crystal structures of compounds **1** and **3** were determined from single crystal X-ray diffraction data, and the crystal packing for any of the complexes did not show any systematic parallel orientation of any part of the molecules. X-ray structural data for the Ni(II) complexes provided a rationale for the $E_{1/2}$ values obtained in the oxidation processes and for the relative energy of the low-lying excited duplets of the electrogenerated Ni(III) species.

Keywords: Crystal structures; Electrochemistry; EPR; Nickel(II)/(III) complexes; Schiff base complexes

1. Introduction

Nickel(II) complexes with N_2O_2 Schiff base ligands derived from salicylaldehyde have long been used as homogeneous catalysts [1–3]. More recently, the ease of preparation of metal salen-based modified electrodes by oxidative electropolymerisation of metal complexes in poor coordinating solvents has prompted their use in heterogeneous electrocatalysis [4]. Knowledge of the role played by structural/electronic effects to control the redox chemistry of these metal complexes may prove to be critical in the design of new catalysts.

We have been studying the oxidative chemistry of Ni(II) complexes with N_2O_2 Schiff base ligands in solvents with different coordinating strength and have found the oxidation products to be solvent dependent [5–15]. Nickel(II) complexes with salicylaldehyde-based ligands (L) are oxidised in dimethylformamide (DMF) and $(CH_3)_2SO$ by a one-electron metal-centred process to six-coordinate Ni(III) species, formulated as $[Ni^{III}L(solv)_2]^+$ (where solv stands for a solvent molecule) [5–9]. However, in CH_3CN the complexes are oxidatively polymerised at the electrode surface to generate electroactive films [10–15], for which the oxidative behaviour has been shown to be associated with a ligand-centred process of the surface redox couple [11–13]. The complexes [Ni(salen)] and [Ni(saltMe)] (see Scheme 1 for an explanation of the abbreviations used) exhibit in strong coordinating solvents (DMF and $(CH_3)_2SO$) a quasi-reversible diffusion-controlled one-electron transfer process [8], in which the value of $E_{1/2}$ of [Ni(salen)] is less positive (approximately 0.07 V in DMF and 0.09 V in $(CH_3)_2SO$) than that of [Ni(saltMe)], a behaviour suggested to arise

* Corresponding author. Tel: +351-22-608 2890; fax: +351-22-608 2959; e-mail: acfreire@fc.up.pt

0277-5387/00/$ - see front matter
PII S0277-5387(00)00300-4

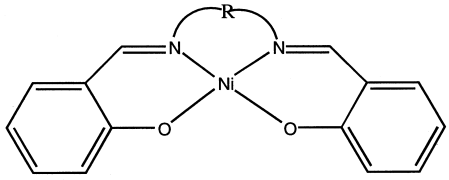

R= -C(CH$_3$)$_2$CH$_2$- [Ni(saldMe)] (1)
R= cyclo-C$_6$H$_{10}$ [Ni(salhd)] (2)
R= -C(CH$_3$)$_2$C(CH$_3$)$_2$- [Ni(saltMe)] (3)
R= -CH$_2$CH$_2$- [Ni(salen)] (4)

Scheme 1.

from steric repulsions imposed on axial binding by the axially oriented methyl groups of the imine bridge [8].

In CH_3CN the electrogenerated polymers exhibit, in the oxidative redox switching, quite different properties in terms of stabilisation; poly[Ni(saltMe)] reveals high stability/durability, and conductivity in CH_3CN (even for very thick polymers) and for a wide potential window [11], a behaviour to be contrasted with that of poly[Ni(salen)], a poor conducting polymer with very low stability [10]. Since these two nickel complexes differ in four methyl substituents of the ethylenimine bridge, we decided to investigate the effect of a smooth increase in the bulkiness of the imine bridge substituents on the solution redox properties of salen-based Ni(II) complexes in $(CH_3)_2SO$ and DMF, and on the redox properties of their electrogenerated polymers in CH_3CN.

The work presented here describes the redox characterisation of [Ni(saldMe)] (**1**) and of [Ni(salhd)] (**2**) in CH_3SO and DMF; the results in CH_3CN will be published elsewhere. The ligand, H_2saldMe, has only two methyl groups in the imine bridge, albeit on the same carbon atom, and the ligand H_2salhd, has the nitrogen atoms bound to two consecutive carbons of a cyclohexane (Scheme 1). These ligands provide intermediate situations between those of H_2salen and H_2saltMe. Cyclic voltammetry and chronoamperometry were used to characterise electrochemically the complexes; chronoamperometric data are also included for [Ni(saltMe)] (**3**). The molecular and crystal structures of [Ni(saldMe)] and [Ni(saltMe)] have been solved and are reported here. Cyclic voltammetric data for [Ni(saltMe)] have been published elsewhere [8], but a brief description of the key features are included to provide a complete and coherent framework for the overall study reported here.

2. Experimental

2.1. Reagents, solvents, ligands and complexes

The solvents for syntheses were of reagent grade and those for electrochemical studies were of analytical grade; all were used as received. All reagents (nickel acetate tetrahydrate, salicylaldehyde, 2-methyl-2,3-propanediamine, 1,2-cyclohexanediamine) were obtained from Aldrich and used as received. Tetraethylammonium perchlorate (TEAP; Fluka, puriss) was kept in an oven at 60°C prior to use. **Caution**: perchlorates are hazards and may explode.

The ligands H_2saldMe, *N*,*N*′-2-methylpropane-2,3-dyil-bis(salicylideneimine), and H_2salhd, *N*,*N*′-1,2-cyclohexyl-1,2-dyil-bis(salicylideneimine), and the respective Ni(II) complexes were prepared by standard methods [16]; in H_2salhd the cyclohexane in the imine bridge exists as a mixture of the *cis* and the *trans* isomers. The synthesis, spectroscopic and cyclic voltammetric studies in DMF and $(CH_3)_2SO$ of the Ni(II) complex with *N*,*N*′-2,3-dimethylbutane-2,3-diyl-bis(salicylideneiminate), [Ni(saltMe)], have been published previously [8]. X-ray quality crystals of [Ni(saldMe)] and [Ni(saltMe)] were obtained by slow evaporation of solutions of the corresponding complexes in CH_3CN–CH_3Cl.

[Ni(saldMe)], $C_{18}H_{18}N_2O_2Ni$. *Anal*. Calc.: C, 61.2; H, 5.1; N, 7.9. Found: C, 61.6; H, 5.2; N, 7.8%. ^{1}H NMR ($CDCl_3$, 298 K, δ): 7.41 (2H, =CH), 7.27–7.01 (6H, aromatic H), 6.59–6.50 (2H, aromatic H), 3.26 (2H, –CH_2), 1.50 (6H, –C(CH_3)$_2$. Electronic spectra (800–250 nm), λ_{max} (ε, mol^{-1} dm^3 cm^{-1}): in $(CH_3)_2SO$, 558 (133), 444 (2460), 410 (5900), 388 (3318), 342 (7146), 321 (7482); in DMF, 559 (137), 444 (3317), 411 (6545), 386 (3614), 344 (7911), 324 (8455).

[Ni(salhd)], $C_{20}H_{20}N_2O_2Ni$. *Anal*. Calc.: C, 63.3; H, 5.3; N, 7.4. Found: C, 63.3; H, 5.2; N, 7.4%. ^{1}H NMR (DMSO-d_6, 298 K, δ): 7.71 (2H, =CH), 7.38–7.34 (2H, aromatic H), 7.20–7.11 (2H, aromatic H), 6.70–6.66 (2H, aromatic H), 6.53–6.50 (2H, aromatic H), 3.11 (4H, –C_6H_{10}), 1.77 (2H, –C_6H_{10}), 1.25 (4H, –C_6H_{10}). Electronic spectra (700–250 nm), λ_{max} (ε, mol^{-1} dm^3 cm^{-1}): in $(CH_3)_2SO$, 557 (133), 443 (3227), 410 (6588), 390 (4152), 345 (7410), 324 (7914); in DMF, 557 (127), 444 (2509), 412 (5717), 392 (3264), 345 (6528), 322 (7443).

Details on the electrosynthesis of Ni(III) complexes and the preparation of their pyridine adducts have been described elsewhere [5,8].

2.2. Physical measurements

Elemental analyses (C, H and N) were performed at the Departamento de Química, Universidade de Aveiro, Portugal. ^{1}H NMR spectra were recorded with a Bruker AC 200 spectrometer at 25°C, using $SiMe_4$ as internal reference. Electronic spectra of Ni(II) complexes were recorded with a Unicam UV2 spectrophotometer at room temperature, in a standard 1-cm quartz cuvette, using solutions of the ligands (1×10^{-5} mol dm^{-3}) or of the metal complexes (1×10^{-3} and 1×10^{-5} mol dm^{-3}) in DMF and $(CH_3)_2SO$. EPR spectra were obtained with a Bruker ESP 300 spectrometer (X-band) at 120 K; the magnetic field was calibrated by using Mn^{2+} in MgO and diphenylpicrylhydrazyl was used as internal reference (dpph; $g=2.0037$). The reported EPR parameters were obtained by spectral simulation using the program WinEPR Simfonia (Bruker) and assuming rhombic

spin hamiltonians; line widths were typically in the range 0.05–0.20 mT.

Electrochemical measurements were performed using an Autolab PGSTAT20 potentiostat/galvanostat. The electrochemical cell used in cyclic voltammetry and in double potential step chronoamperometry was a closed standard three-electrode cell connected to a solution reservoir through a Teflon tube. A Pt disk electrode with an area of 0.0314 cm^2 was used as the working electrode, a Pt gauze electrode as the counter electrode and an Ag/AgCl (1 mol dm^{-3} NaCl) as reference electrode. The ferrocene/ferrocinium (Fc/Fc) redox couple was used as internal standard: under the experimental conditions used, $E_{1/2}$ for the Fc/Fc^+ couple was 0.48 and 0.45 V in DMF and $(CH_3)_2SO$, respectively. Prior to use, the Pt working electrode was polished with an aqueous suspension of 0.05-μm alumina (Buehler) on a Master-Tex (Buehler) polishing pad, then rinsed with water and acetone and dried in an oven. All solutions were de-areated and delivered to the cell by a stream of argon. For cyclic voltammetry, scan rates in the interval 0.005–1.0 V s^{-1} were used, and the potential limits were 0.0 and 1.3 V. For chronoamperometry the potential was stepped from 0.0 V to E_1 and back to 0.0 V. After each step the potential was held for 20 s. The applied potentials E_1 were the same for all complexes in DMF and equal to 1.0 V; in $(CH_3)_2SO$ they were 0.93, 0.90 and 1.0 V for [Ni(saldMe)], [Ni(salhd)] and [Ni(saltMe)], respectively.

Electrolysis were carried out at controlled potential, at a value 0.1 V higher than the anodic peak potential. A three-electrode cell was used, with a Pt gauze as the working electrode, a Pt foil as counter electrode and an Ag/AgCl (1 mol dm^{-3} NaCl) as reference electrode.

2.3. Crystallography

Data were collected at room temperature for [Ni(saldMe)] on an Enraf Nonius TURBOCAD4 diffractometer with a copper rotating anode and for [Ni(saltMe)] on an Enraf Nonius MACH3 diffractometer with Mo graphite monochromatised radiation. Data reduction, Lorentz, polarisation and empirical absorption corrections were made using the CAD4 software package.

For both complexes the positions of the nickel atoms were obtained from a three-dimensional Patterson synthesis. Three molecules were found in the asymmetric unit of compound [Ni(saltMe)], while only one molecule was refined in complex [Ni(saldMe)]. All the non-hydrogen atoms were located in subsequent difference Fourier maps, and were refined, on F^2, with anisotropic thermal motion parameters. The hydrogen atoms were inserted in calculated positions and refined isotropically riding with the parent carbon atom. Details for data collection and for structure refinement are presented in Table 1.

Structure solution and refinement were done with SHELXS-86 [17] and SHELX-97 [18], and all molecular diagrams were drawn with the program ORTEP III [19]. Atomic scattering factors and anomalous scattering terms

Table 1
Crystal data and structure refinement for [Ni(saldMe)] and [Ni(saltMe)]

Identification code	[Ni(saldMe)]	[Ni(saltMe)]
Empirical formula	$C_{18}H_{18}N_2NiO_2$	$C_{20}H_{22}N_2NiO_2$
Formula weight	353.09	381.11
Temperature (K)	293(2)	293(2)
Wavelength (Å)	1.54184	0.71069
Crystal system	orthorhombic	monoclinic
Space group	*Pcab*	$P2_1/a$
Unit cell dimensions		
a (Å)	11.521(3)	11.1850(10)
b (Å)	15.973(4)	21.640(3)
β (°)		91.040(10)
c (Å)	17.414(4)	22.245(2)
Volume ($Å^3$)	3204.6(14)	5383.4(10)
Z	8	12
Calc. density (Mg m^{-3})	1.464	1.411
Absorption coefficient (mm^{-1})	1.671	1.096
$F(000)$	1472	2400
Theta range for data collection (°)	5.08–72.60	1.83–27.00
Index ranges	$-14 \le h \le 0$; $-19 \le k \le 0$; $-21 \le l \le 0$	$-14 \le h \le 14$; $-27 \le k \le 1$; $-28 \le l \le 28$
Reflections collected/unique	3182/3182 ($R_{int} = 0.0000$)	24706/11732 ($R_{int} = 0.0609$)
Completeness to 2θ (%)	72.60, 96.5	27.00, 97.2
Refinement method	full-matrix least-squares on F^2	full-matrix least-squares on F^2
Data/restraints/parameters	3182/0/205	11732/0/739
Goodness-of-fit on F^2	1.105	1.033
Final R indices [$I > 2\sigma(I)$]	$R1 = 0.0535$; $wR2 = 0.1494$	$R1 = 0.0586$; $wR2 = 0.1034$
R indices (all data)	$R1 = 0.0679$; $wR2 = 0.1674$	$R1 = 0.1278$; $wR2 = 0.1344$
Largest difference peak and hole (e $Å^{-3}$)	0.272 and −1.003	0.925 and −0.644

were taken from International Tables for Crystallography [20].

3. Results and discussion

3.1. Spectroscopic characterisation

Ni(II) complexes with the ligands H_2saldMe and H_2salhd show electronic spectra in DMF and $(CH_3)_2SO$ that are very similar to those of [Ni(saltMe)] and of other Ni(II) Schiff base complexes derived from salicylaldehyde, both in solution and in solid. They are characteristic of square planar low-spin Ni(II) complexes [21]; typically the spectra exhibit a low-intensity broad brand at $\lambda_{max} \approx 550$–560 nm ($\varepsilon \approx 125$–135 mol^{-1} dm^3 cm^{-1}) assigned to transitions from the four low-lying orbitals, which is superimposed on a group of high-intensity charge transfer bands at higher energies ($\lambda <$ 440 nm, $\varepsilon \approx 2500$–500 mol^{-1} dm^3 cm^{-1}). The similarity between the spectra in both solvents and in the solid indicates that no effective coordination of solvent molecules took place in any of the solvents.

3.2. Molecular structure

Molecular structure of complexes [Ni(saldMe)] and [Ni(saltMe)] are depicted in Figs. 1 and 2; relevant bond lengths and bond angles and the most relevant torsion angles are listed in Table 2. The same numbering scheme was used for the three independent molecules of [Ni(saltMe)].

In both compounds the coordination geometry around the nickel atom is roughly square planar, with the ligands bound through two nitrogen and two oxygen atoms in a *cis* configuration, but with the four N_2O_2 atoms distorted in a tetrahedral fashion.

The maximum deviation from planarity of the coordinated atoms in [Ni(saltMe)] are 0.074(2), 0.084(2) and 0.099(2) Å for molecules A, B and C, respectively, while the nickel atom is 0.018(2) Å out of that plane for molecule A, and 0.016(2) Å for molecules B and C. In [Ni(saldMe)], the coordination atoms are more distorted towards a tetrahedron, with a maximum deviation from planarity of 0.124(1) Å and with the nickel atom 0.013(1) Å out of the plane. The values of maximum deviation from planarity compare with those found for the two independent molecules of [Ni(1*R*,2*R*(-)salhd)] [22], which are 0.057 Å for molecule 1 and 0.088 Å for molecule 2; however, in this molecule the nickel atom lies practically within the coordination plane (−0.0096 and −0.0042 Å, respectively). The values of maximum deviation from planarity also compare with those found for *N*,*N*′-1,2-*cis*-cyclohexane-1,2-diyl-bis(2-hydroxyacetophenonylidene-iminate)nickel(II), [Ni(α,α′-Me_2-salhd)], for which the deviation is 0.076 Å and the nickel atom is 0.018 Å out of the plane [7]. It must be pointed that [Ni(salhd)] exists in solution as a mixture of isomers and it is to be expected that they present a comparable deviation

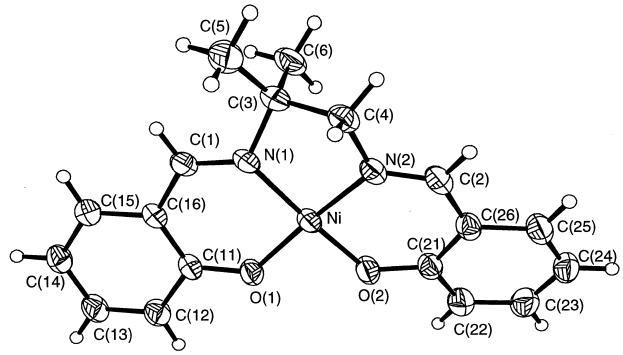

Fig. 1. Molecular diagram with atomic labelling scheme for [Ni(saldMe)]. Ellipsoids at 40% probability level [19,38].

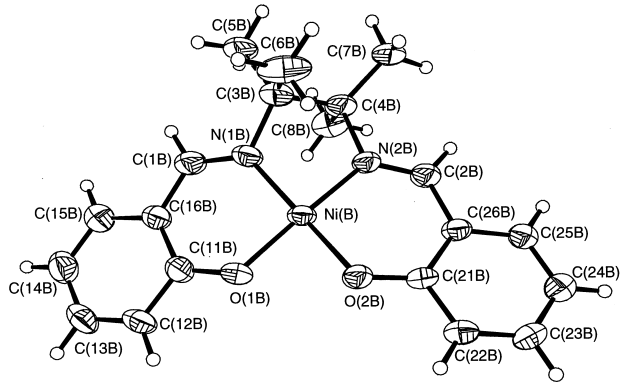

Fig. 2. Molecular diagram with atomic labelling scheme for molecule B of [Ni(saltMe)]. Ellipsoids at 40% probability level [19,38].

from planarity. In contrast, the structure of the compound with no substituents in the imine bridge, [Ni(salen)], is almost planar; maximum deviation from planarity of 0.023 Å and with the nickel atom 0.0056 Å out of the plane [23].

The configuration of the three independent molecules of [Ni(saltMe)] is asymmetric umbrella, with NCCN torsion angles of 20(1)° for molecule A, −43.9(6)° for molecule B and −46.7(5)° for molecule C; the conformations of the imine bridge are thus *cis*, *gauche* and *gauche*, respectively. Deviations of the imine bridge atoms, C3 and C4, from the NiN_2O_2 plane are −0.02(1) and −0.19(1) Å (molecule A), −0.619(8) and 0.097(7) Å (molecule B) and −0.300(7) and 0.507(7)° (molecule C). The values of the torsion angle for molecules B and C are of the same order of magnitude as those observed in the homologous ligand derived from naphthaldehyde, [Ni(naptMe)], for which the value is 47.5(5)° [6].

The configuration of the [Ni(saldMe)] molecules is an asymmetric umbrella but with the two aldehyde moieties twisted. The NCCN torsion angle is 39.6(5)°, smaller than those found in the two crystallographic independent molecules in the similar complex *N*,*N*′-2-methylpropane-2,3-diyl-bis(3-hydroxysalicylideneiminate)nickel(II), [Ni(3-HO-saldMe)], [24], which are 44(1) and 45(1)°. The two carbon atoms, C3 and C4, in [Ni(saldMe)] are below and above the NiO_2N_2 coordination plane with a quasi-symmetric displacement, −0.365(5) and +0.341(5) Å, respectively.

Table 2
Selected bond lengths (Å), bond angles (°) and torsion angles for [Ni(saldMe)] and [Ni(saltMe)]

	[Ni(saldMe)]	[Ni(saltMe)]		
		A molecule	B molecule	C molecule
Ni–O(1)	1.836(2)	1.844(3)	1.844(3)	1.829(3)
Ni–O(2)	1.845(2)	1.839(3)	1.842(3)	1.835(3)
Ni–N(2)	1.847(2)	1.837(4)	1.846(4)	1.842(4)
Ni–N(1)	1.853(3)	1.843(4)	1.838(4)	1.858(4)
N(1)–C(1)	1.291(4)	1.290(6)	1.290(6)	1.279(6)
N(1)–C(3)	1.502(4)	1.494(6)	1.494(6)	1.499(6)
O(1)–C(11)	1.310(4)	1.297(5)	1.305(6)	1.307(6)
N(2)–C(2)	1.292(4)	1.287(6)	1.278(6)	1.301(6)
N(2)–C(4)	1.462(4)	1.502(7)	1.523(6)	1.498(6)
O(2)–C(21)	1.318(4)	1.297(5)	1.302(5)	1.317(6)
C(1)–C(16)	1.434(4)	1.418(7)	1.427(6)	1.425(7)
C(3)–C(4)	1.517(5)	1.298(9)	1.479(8)	1.544(7)
C(3)–C(6)	1.524(5)	1.875(10)	1.601(8)	1.545(7)
C(3)–C(5)	1.525(5)	1.477(7)	1.521(7)	1.521(7)
C(2)–C(26)	1.422(5)	1.429(6)	1.427(6)	1.433(7)
O(1)–Ni–O(2)	84.41(10)	83.85(14)	84.64(14)	83.79(16)
O(1)–Ni–N(2)	173.07(11)	174.3(2)	173.80(17)	174.75(17)
O(2)–Ni–N(2)	94.77(11)	95.61(16)	95.42(15)	95.17(17)
O(1)–Ni–N(1)	95.34(10)	95.76(16)	94.62(16)	95.60(16)
O(2)–Ni–N(1)	171.63(12)	176.46(17)	175.72(18)	172.88(17)
N(2)–Ni–N(1)	86.47(11)	85.13(18)	85.77(17)	86.07(17)
C(1)–N(1)–C(3)	119.2(3)	120.3(4)	121.4(4)	121.4(4)
C(1)–N(1)–Ni	126.1(2)	125.7(3)	126.9(3)	125.0(4)
C(3)–N(1)–Ni	114.0(2)	113.8(3)	111.5(3)	113.2(3)
C(11)–O(1)–Ni	127.52(19)	126.7(3)	126.1(3)	127.8(3)
C(2)–N(2)–C(4)	120.1(3)	122.3(4)	120.9(4)	122.4(5)
C(2)–N(2)–Ni	126.8(2)	125.1(3)	125.3(3)	125.2(4)
C(4)–N(2)–Ni	112.7(2)	112.6(4)	112.8(3)	112.4(3)
C(21)–O(2)–Ni	127.4(2)	126.4(3)	126.8(3)	126.0(4)
N(1)–C(1)–C(16)	125.0(3)	125.9(5)	124.3(5)	126.5(5)
C(11)–C(16)–C(1)	121.9(3)	121.5(4)	121.5(5)	121.5(5)
O(1)–C(11)–C(16)	123.7(3)	123.8(4)	124.3(4)	123.6(5)
O(1)–C(11)–C(12)	118.8(3)	118.7(4)	118.5(5)	118.4(5)
C(16)–C(11)–C(12)	117.5(3)	117.5(4)	117.1(5)	118.1(5)
N(1)–C(3)–C(4)	103.8(3)	112.1(5)	103.9(4)	103.9(4)
N(1)–C(3)–C(6)	107.0(3)	99.9(5)	107.8(5)	108.0(4)
C(4)–C(3)–C(6)	111.3(3)	86.9(7)	105.7(5)	110.6(4)
N(1)–C(3)–C(5)	113.6(3)	115.6(5)	114.0(5)	112.2(4)
C(4)–C(3)–C(5)	109.5(3)	127.1(6)	113.7(5)	113.7(4)
C(6)–C(3)–C(5)	111.4(3)	105.5(6)	111.0(5)	108.2(5)
N(2)–C(2)–C(26)	125.3(3)	126.0(4)	125.5(4)	125.2(5)
C(21)–C(26)–C(2)	121.5(3)	120.7(4)	121.7(4)	121.7(5)
O(2)–C(21)–C(22)	118.2(3)	119.4(4)	119.7(4)	118.2(6)
O(2)–C(21)–C(26)	123.8(3)	124.3(4)	123.6(4)	123.5(5)
N(2)–C(4)–C(3)	108.7(3)	112.9(6)	106.0(4)	103.1(4)
N(1)–C(3)–C(4)–N(2)	39.6(3)	19.6(13)	−43.9(6)	−46.7(5)

The maximum deviation from planarity of the coordinated atoms (and the distance of the nickel atom to the equatorial plane) in similar molecules which have ethylene-based bridges without substituents or aromatic bridges are 0.033 Å (0.0073 Å) in [Ni(α,α′-Me_2salen)] [7], 0.023 Å (0.0056 Å) in [Ni(salen)] [23], 0.013 Å in [Ni(saloph)] [25], 0.039 Å (0.0078 Å) in [Ni(3,5-Cl_2salophen)] [7] and 0.01 Å in [Ni(napen)] [26]. We can conclude, when comparing the above values with those of [Ni(saldMe)], [Ni(1*R*,2*R*-(-)salhd)] and [Ni(saltMe)], that the observed distortions are mainly due to the bulkiness of the substituents in the imine bridge. The presence of these bulky substituents imposes severe steric requirements due to interactions between the hydrogen atoms, and consequently the three molecules [Ni(saldMe)], [Ni(saltMe)] and [Ni(salhd)] are quite distorted.

Another key result that emerged from the molecular structures is that one methyl group in [Ni(saldMe)] is oriented perpendicular to the equatorial plane, and that two methyl groups in [Ni(saltMe)] are oriented perpendicular to the

equatorial plane and in opposite directions. No crystal structure is known for [Ni(salhd)] with the cyclohexane in the *cis* form, but recalling that of [Ni(α,α′-Me_2salhd)] it is to be expected the ring to be also axially oriented.

Regarding the Ni–O and Ni–N bonding distances (Table 2), they are comparable to those observed in Schiff base complexes with identical coordination spheres [6,7,23–29] and are within the average values found in a Cambridge Structural Database search [28,29] for compounds having two carbon atoms in the imine bridge. The relative values of Ni–O and Ni–N bond lengths do not follow any pattern and no trend could be established between their values and any of the parameters used to characterise molecular distortion.

3.3. Crystal packing

The packing of both [Ni(saldMe)] and [Ni(saltMe)] do not show any Ni···Ni intermolecular distance below 3.5 Å. In the packing of [Ni(saldMe)] the shorter Ni···Ni interaction is 4.463 Å, and for [Ni(saltMe)] the existence of three independent molecules with such different orientations in the asymmetric unit prevents shorter interactions in the crystal packing. The shorter ones, 5.561 and 6.471Å, are between the nickel atom of molecule A and the nickel atoms of molecules B and C. Actually, the close intermolecular interactions between molecule A and the surrounding molecules in the unit cell explain the different conformation found for this molecule.

3.4. Cyclic voltammetry

3.4.1. Ligands

The three ligands, H_2saldMe, H_2salhd and H_2saltMe, are irreversibly oxidised in both solvents; the respective anodic peak potentials (scan rate 0.01 V s^{-1}) are approximately 1.22, 1.26 and 0.88 V in DMF, and 1.17, 1.15 and 0.84 V in $(CH_3)_2SO$. With increasing scan rates all ligands show a positive peak potential shift, as well as an increase in current intensity. Although no comparison between the potential peak values of the three ligands can be made due to the irreversible nature of charge transfer, it should be noted that the peak potential pattern for H_2saltMe is quite different from that of the other ligands.

3.4.2. Nickel complexes

Cyclic voltammetric data are summarised in Table 3. The results for [Ni(saltMe)] have been published elsewhere [8], and this complex shows in both solvents a quasi-reversible oxidation of Ni(II) to Ni(III). The cyclic voltammograms of [Ni(saldMe)] and [Ni(salhd)] are solvent dependent; in DMF in the potential range used they exhibit one anodic peak and the corresponding cathodic peak. The values of $E_{1/2}$ (vs. Ag/AgCl) are very similar and the anodic–cathodic peak potential separations, for the lowest scan rates used, are comparable to that of Fc^+/Fc couple, but somewhat higher for fast sweep rates. The ratio i_{pc}:i_{pa} was found to decrease with increasing scan rates.

The behaviour of [Ni(saldMe)] and [Ni(salhd)] in $(CH_3)_2SO$ is more intricate, since the voltammograms are dependent on scan rate. At low scan rates (0.005–0.02 V s^{-1}), two anodic waves, E_{pa}(I) and E_{pa}(II), but only one cathodic wave, which is related to the first anodic process (E_{pc}(I)), could be detected (Fig. 3 and Table 3). As the scan rate increases, a positive shift in E_{pa}(I) and E_{pa}(II) (larger for the latter process) and an increase in peak current (smaller for the latter process) are observed; furthermore, for scan rates faster than 0.05 V s^{-1} only the first anodic wave and the corresponding cathodic wave could be observed, as shown in Fig. 3. The ratio i_{pc}:i_{pa} (Table 3) for the first process is somewhat larger than 1 for low scan rates, but smaller than 1 for the highest scan rates.

For [Ni(saldMe)] and [Ni(salhd)] in the two solvents, the dependence of i_p with $\nu^{1/2}$ was found to be linear at low scan rates, but to deviate from linearity with increasing sweep rate. By coupling these results with the observations that, with increasing scan rate, the ratios i_{pc}:i_{pa} become smaller than 1 and the anodic–cathodic peak potential separation (ΔE) becomes larger than the values for Fc^+/Fc, it becomes clear that the rate of the electron transfer, relative to that of the mass transport, is insufficient to maintain the nernstian

Table 3
Cyclic voltammetric data for Ni(II) complexes in DMF and $(CH_3)_2SO$ (0.1 mol dm^{-3} TEAP) [a]

Complex	ν (V s^{-1})	In DMF					In $(CH_3)_2SO$					
		E_{pa}	E_{pc}	ΔE	$E_{1/2}$	i_{pc}:i_{pa}	E_{paI}	E_{paII}	E_{pcI}	ΔE	$E_{1/2}$	i_{pc}:i_{pa} [b]
[Ni(salhd)]	0.01	0.87	0.78	0.08	0.83	1.02	0.77	0.91	0.69	0.08	0.73	1.05
	1	0.92	0.73	0.19	0.82	0.68	0.87	[c]	0.39	0.48	[d]	0.65
[Ni(saldMe)]	0.01	0.85	0.78	0.07	0.82	1.02	0.76	0.88	0.70	0.06	0.73	1.05
	1	0.89	0.74	0.15	0.82	0.75	0.81	[c]	0.63	0.18	[d]	0.80
[Ni(saltMe)]	0.01	0.94	0.84	0.10	0.89	1.00	0.86	–	0.78	0.08	0.82	0.93
	1	0.94	0.85	0.09	0.90	0.97	0.89	–	0.75	0.14	0.82	0.78

[a] All potentials are referred to Ag/AgCl (1 mol dm^{-3} NaCl).
[b] Refers to process denoted as (I).
[c] The anodic wave is not detected at high scan rates.
[d] Electrochemical process with a high degree of irreversibility.

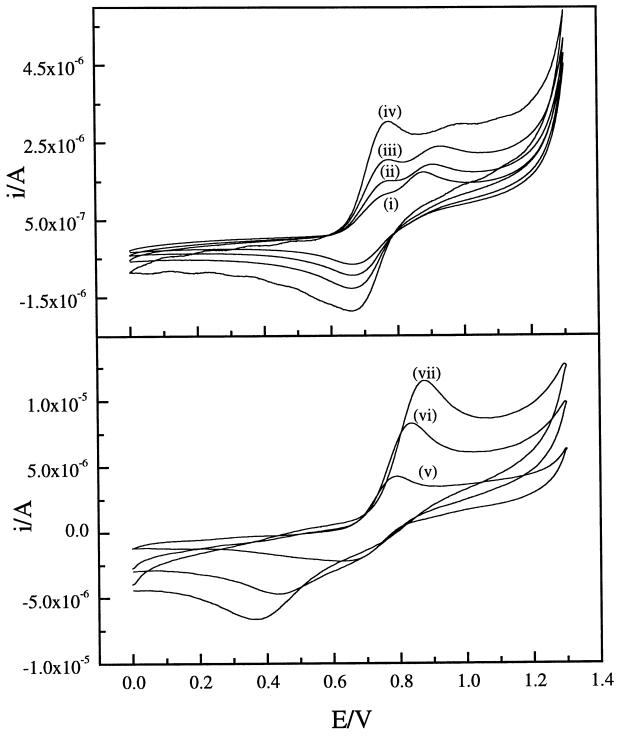

Fig. 3. Cyclic voltammograms of [Ni(salhd)] in 0.1 mol dm^{-3} TEAP–$(CH_3)_2SO$ between 0.00 and 1.30 V at different scan rates: (i) 0.005, (ii) 0.010, (iii) 0.020, (iv) 0.050, (v) 0.100, (vi) 0.500, (vii) 1.00 V s^{-1}.

equilibrium at the electrode surface. The one-electron charge transfer process is thus reversible and diffusion controlled at low scan rates, whereas at high scan rates a transition to a quasi-reversible mixed (kinetic and diffusion) controlled process must take place [30].

The oxidation of several N_2O_2 salicylaldehyde-derived Schiff base Ni(II) complexes has been shown to occur with a concomitant axial coordination of solvent molecules, and this step proved to be decisive in the overall charge transfer process, as it controls the final oxidised products and the $E_{1/2}$ values [5–15]. A similar solvent dependence is also operative in the oxidation process of [Ni(salhd)] and [Ni(saldMe)], as can be gathered by noting that their $E_{1/2}$ values are less positive in $(CH_3)_2SO$, the strong coordinating solvent used.

The $E_{1/2}$ values for [Ni(salhd)] and [Ni(saldMe)] in each solvent are similar, albeit slightly more positive than that of [Ni(salen)] [$E_{1/2}$ (DMF) = 0.81 V and $E_{1/2}$ ($(CH_3)_2SO$) = 0.70 V; scan rate 0.01 V s^{-1}] and less positive than that of [Ni(saltMe)]. To account for this behaviour, it must be pointed out that introduction of substituents in the imine bridge not only affects the electronic properties of the complex, but also may impose steric constraints on axial coordination. Electron-donating substituents (methyl groups and the cyclohexyl) are expected to decrease the values of $E_{1/2}$, and as such their $E_{1/2}$ values would be expected to be less positive than those of [Ni(salen)]. However, the values obtained were more positive, an indication that steric constraints play a more important role than electronic effects in the solution stability of the electrogenerated Ni(III) species. The X-ray structure of [Ni(saldMe)] shows one methyl group oriented towards one axial position which thus will interact directly with one axially bound solvent molecule in the oxidised species, weakening the bond to the metal with the consequent destabilisation of Ni(III) complexes. This explanation also holds for [Ni(saltMe)], for which two methyl groups of the imine bridge are directed towards two opposite axial positions thus weakening axial coordination of the two solvent molecules in the Ni(III) complexes. Therefore [Ni(saltMe)] exhibits, as expected, the more positive $E_{1/2}$ values for the series of complexes studied. Although no crystal structure for the *cis* isomer of [Ni(salhd)] is known, the preceding discussion suggests that in this isomer the cyclohexane ring must hinder axial coordination and must influence markedly its electrochemical responses.

A caveat to the above discussion is that structural data were obtained in the solid state. In solution, where solid states effects are absent, it is not possible to rule out the existence of other conformations of [Ni(saldMe)] and [Ni(salhd)], and thus the two anodic processes observed at low scan rates in $(CH_3)_2SO$ may be due to the oxidation of complexes in different conformations, one of which does not allow stabilisation of Ni(III) species.

3.5. Chronoamperometry

In both solvents the current–time responses in chronoamperometric experiments for [Ni(saldMe)], [Ni(salhd)] and [Ni(saltMe)], depicted as i versus $t^{-1/2}$ (Cottrell representation [30]), are straight lines that exhibit small deviations from linearity for long periods, particularly in the reduction step (typically longer than 6 s for the oxidation and 2 s for the reverse step). These deviations from linearity suggest a change from a diffusion-controlled process to a mixed controlled process [30], as has been inferred from cyclic voltammetry in $(CH_3)_2SO$. By using the linear region of the Cottrell equation, the diffusion coefficients for oxidation ($D_{CA}{}^{oxi}$) and the reverse step ($D_{CA}{}^{red}$) were calculated and are summarised in Table 4. The values for $D_{CA}{}^{oxi}$ are of the same magnitude as those obtained for the oxidation of [Ni(salen)] and [Co(salen)] using the Randles–Sevcik equation [31].

Table 4
Values of D_{CA} obtained using the Cottrell equation

Complex	$(CH_3)_2SO$		DMF	
	Step (V)	$10^6 D_{CA}$ (cm^2 s^{-1})	Step (V)	$10^6 D_{CA}$ (cm^2 s^{-1})
[Ni(saldMe)]	0.0→0.93	4.00	0.0→1.0	9.20
	0.93→0.0	3.66	1.0→0.0	8.91
[Ni(salhd)]	0.0→0.90	3.68	0.0→1.0	8.91
	0.90→0.0	3.10	1.0→0.0	8.58
[Ni(saltMe)]	0.0→1.0	2.98	0.0→1.0	8.35
	1.0→0.0	2.65	1.0→0.0	7.35

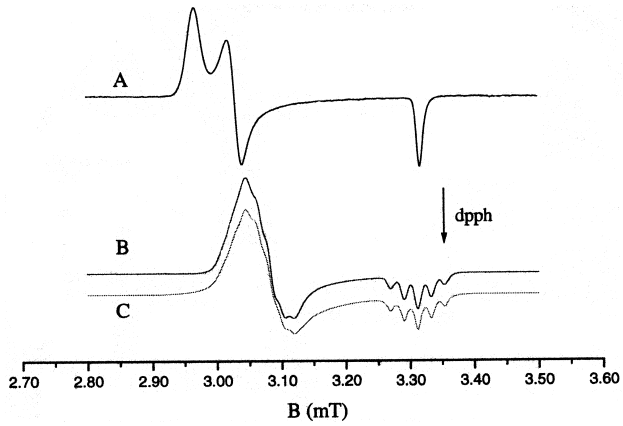

Fig. 4. Frozen-solution X-band EPR spectra at −140°C of (A) an electrochemically oxidised solution of [Ni(saldMe)] in DMF, (B) the corresponding pyridine adduct, and its simulation (C).

Analysis of D_{CA} shows that: (1) the values in DMF are higher than those obtained in $(CH_3)_2SO$, and (2) the values decrease in both solvents in the order [Ni(saldMe)] > [Ni(salhd)] > [Ni(saltMe)]. Solvent dependence can easily be accounted for by differences in solvent viscosity [30,31]: the complexes have smaller D_{CA} values in the solvent with higher viscosity, $(CH_3)_2SO$. No straightforward explanation can be invoked for the differences in D_{CA} for the complexes; we note, however, that the smallest value is obtained for the complex with the longest axial bonds ($[Ni(saltMe)(solv)_2]^+$ (see EPR section, below), and that the average size of the Ni(III) complexes may be the key factor in controlling diffusion.

3.6. Electrolysis and EPR characterisation of the oxidised solutions

Electrochemical oxidation of [Ni(saldMe)] and [Ni(salhd)] in DMF and $(CH_3)_2SO$ proceeds as that of [Ni(saltMe)] and [Ni(salen)] [8], with a solution colour change from reddish to dark brown. Frozen-solution EPR spectra of electrolytically generated nickel complexes are similar in both solvents, and show the rhombic symmetry and the large *g* tensor anisotropy typically associated with metal-centred oxidised species (Fig. 4A). The spectra exhibit no hyperfine splittings and are similar to those of oxidised solutions of [Ni(saltMe)], [Ni(salen)] [8] and other electrogenerated Ni(III) Schiff base complexes derived from salicylaldehyde [5–7]. The oxidised complexes can thus be formulated as six-coordinate, with two solvent molecules bound axially, $[Ni(L)(solv)_2]^+$, and with the metal centre in a low-spin $^2A_1$ (d_{z^2}) ground state. In the absence of EPR crystal data for the Ni(III) complexes studied, the observed similarity between their *g* features and those of analogous Ni(III) compounds [5–9] can be extended to support the following orientation scheme for the tensor axes of the nickel complexes: $g_1 = g_x$, $g_2 = g_y$, $g_3 = g_z$, where g_1 an g_3 refer to the lowest and highest magnetic field *g* values, respectively. EPR data for Ni(III) species in DMF and $(CH_3)_2SO$ are summarised in Table 5; for comparison the values for $[Ni(salen)(X)_2]^+$ and $[Ni(saltMe)(X)_2]^+$ are also included.

In order to obtain more information on the effect of the imine bridge substituents on the electronic properties of six-coordinate Ni(III) species, the EPR characterisation was extended to compounds with axially bound pyridine molecules. Upon addition of pyridine to freshly prepared solutions of electrogenerated Ni(III) complexes in DMF at temperatures just above the softening point of the frozen glass, new Ni(III) species are formed, as can be inferred from their frozen-solution EPR spectra (Fig. 4B). These are of rhombic type, although with less rhombicity than the parent complexes, have smaller values of g_{av} (2.140–2.144) and exhibit hyperfine couplings in all *g* regions. The existence of one

Table 5
EPR parameters for $[Ni(L)(X)_2]^+$ complexes

Complex	Experimental values					Coefficients [a]			Energy of excited state (cm^{-1})		
	g_x	g_y	g_z	g_{av} [b]	Δ_{xy}	C_1	C_2	C_3	$\Delta(^2B_1)$	$\Delta(^2A_2)$	ΔQ [c]
$[Ni(salen)(dmf)_2]^+$ [d]	2.266	2.222	2.021	2.170	0.044	0.0343	0.0424	0.1075	11465	9275	3658
$[Ni(salen)(Me_2SO)_2]^+$ [d]	2.256	2.216	2.020	2.164	0.040	0.0334	0.0399	0.1045	11774	9856	3763
$[Ni(salen)(py)_2]^+$ [d]	2.201	2.172	2.021	2.131	0.029	0.0251	0.0298	0.1096	15667	13196	3588
$[Ni(salhd)(dmf)_2]^+$	2.267	2.220	2.027	2.171	0.047	0.0330	0.0405	0.1202	11930	9707	3273
$[Ni(salhd)(Me_2SO)_2]^+$	2.264	2.223	2.026	2.171	0.041	0.0336	0.0402	0.1181	11700	9780	3330
$[Ni(salhd)(py)_2]^+$	2.208	2.182	2.030	2.140	0.026	0.0257	0.0299	0.1236	15310	13150	3181
$[Ni(saldMe)(dmf)_2]^+$	2.268	2.220	2.027	2.172	0.048	0.0330	0.0407	0.1202	11930	9667	3271
$[Ni(saldMe)(Me_2SO)_2]^+$	2.263	2.223	2.026	2.171	0.040	0.0336	0.0400	0.1180	11700	9821	3332
$[Ni(saldMe)(py)_2]^+$	2.213	2.190	2.030	2.144	0.023	0.0271	0.0309	0.1230	14270	12740	3196
$[Ni(saltMe)(dmf)_2]^+$ [d]	2.265	2.224	2.020	2.170	0.041	0.0348	0.0414	0.1053	11300	9499	3734
$[Ni(saltMe)(Me_2SO)_2]^+$ [d]	2.254	2.226	2.020	2.167	0.028	0.0351	0.0396	0.1047	11204	9931	3756
$[Ni(saltMe)(py)_2]^+$ [d]	2.214	2.186	2.022	2.141	0.028	0.0278	0.0324	0.1060	14146	12137	3710

[a] Obtained from McGarvey equations; see text.
[b] The value of g_{av} was calculated as $(g_x + g_y + g_z)/3$.
[c] Difference between the average energy of the quartet states and the ground state.
[d] From [8].

Table 6
^{14}N superhyperfine coupling constants and spin densities for $[NiL(py)_2]^+$ complexes

Complex	Experimental superhyperfine coupling [a]					Anisotropic superhyperfine tensor		Spin densities on ^{14}N			λ^2
	A_x	A_y	A_z	$A_\perp$ [b]	A_{iso} [c]	$A_{xx,yy}$	A_{zz}	C^2_{2s}	C^2_{2p}	Total [d] (%)	
$[Ni(salen)(py)_2]^+$ [e]	1.65	1.76	2.14	1.71	1.85	−0.15	0.28	0.033	0.084	23.4	2.5
$[Ni(salhd)(py)_2]^+$	1.70	1.65	2.13	1.68	1.83	−0.15	0.29	0.033	0.088	24.1	2.7
$[Ni(saldMe)(py)_2]^+$	1.85	1.75	2.15	1.80	1.92	−0.12	0.22	0.034	0.067	20.2	1.9
$[Ni(saltMe)(py)_2]^+$ [e]	1.82	1.63	2.14	1.72	1.86	−0.14	0.27	0.033	0.080	22.7	2.4

[a] The A values are expressed in mT.
[b] $A_\perp$ was calculated as $(A_x+A_y)/2$.
[c] A_{iso} could not be obtained for the adducts; instead it was calculated from $(A_x+A_y+A_z)/3$.
[d] Spin density delocalized onto the two axial nitrogen atoms.
[e] From [8].

well-resolved quintuplet ($A=2.15$–2.13 mT) in the region of higher magnetic field and of two non-resolved quintuplets in the other g regions, implies that solvent molecules have been substituted by two pyridines (^{14}N; $I=1$) and that the resulting Ni(III) complexes have unequivocally a low-spin $^2A_1$ (d_{z^2}) ground state. The similarity between the g pattern of these species with those of the parent complex supports the same orientation scheme for the g tensor of the pyridine adducts.

No EPR signals were detected in fluid solutions of pyridine–DMF or in frozen solution of pyridine adducts in $(CH_3)_2SO$, as has also been observed for the homologous complexes with H_2salen and H_2saltMe ligands, a consequence of the very fast decomposition rate of the pyridine adducts in fluid solutions [5,8,9,32]. EPR parameters for $[Ni(L)py_2]^+$ are summarised in Tables 5 and 6; values for similar complexes with salen and saltMe are also included.

3.7. Electronic structure of the Ni(III) species

Analysis of the EPR parameters using the model developed by McGarvey for d^7 systems with an $^2A_1$ (d_{z^2}) ground state [33], in conjunction with the approximation suggested by Labause and Raynor [34,35], can provide information on the electronic structure of Ni(III) species. A full description of this analysis is described elsewhere [5,8,9] and its application allows an estimate of the energy of excited doublet states $\Delta(^2B_1)$ and $\Delta(^2A_2)$ and the average energy of the quartet states ΔQ, provided the values of complex spin orbit coupling constants (ξ) are known. We have used the ξ values of $[Ni(saltMe)((CH_3)_2SO)_2]^+$ and $[Ni(salen)((CH_3)_2SO)_2]^+$, which were found to be 55% of the free ion [8,36]. In Table 5 are included the values for $\Delta(^2B_1)$, $\Delta(^2A_2)$ and ΔQ for $[Ni(L)(DMF)_2]^+$, $[Ni(L)((CH_3)_2SO)_2]^+$ and $[Ni(L)(py)_2]^+$.

Analysis of data in Table 6 failed to reveal any correlation between the energy of the excited quartets and axial ligation. The energy of the doublet states does not change significantly when the solvent is varied from DMF to $(CH_3)_2SO$, but the axial coordination of pyridine induces a significant increase in the energy of the doublets, as a result of the strong interaction of the pyridine lone pair with the d_{z^2} orbital. This increase lowers the value of the McGarvey coefficients, C_2 and C_1, and using the g factor equations neglecting second-order terms, $g_x=2.0023+6C_2$ and $g_y=2.0023+6C_1$ [5,8,9], a decrease in g_x and g_y is predicted, as was actually observed.

Analysis of data in Table 5 reveals also that for the same axial coordinate molecule (X = DMF, $(CH_3)_2SO$ and py), the energy of the excited doublets decreases in the order $[Ni(salen)(X)_2]^+ > [Ni(salhd)(X)_2]^+ \geq [Ni(saldMe)(X)_2]^+ > [Ni(saltMe)(X)_2]^+$. This ordering reflects the strength of the axial ligation/axial bond length and thus we can deduce that axial bond lengths in the Ni(III) complexes with saltMe are the weakest (longest), and that those of salen complexes are the strongest (shortest), with the other complexes exhibiting intermediate and similar bond lengths. These observations correlate with the sequence of $E_{1/2}$ values, and reflects mainly, as mentioned above, steric interactions of the imine bridge substituents with the axially bound molecules in Ni(III) complexes.

3.7.1. Nitrogen hyperfine tensor and spin density on nitrogen atoms of axial bound pyridines

The 2s and 2p spin densities, the ratio p:s ($\lambda^2=C^2_{2p}/C^2_{2s}$) and the total spin density delocalised onto the axially bounded pyridine have been calculated by procedures described elsewhere [5,8,9,37] and are reported in Table 6. The values of C^2_{2s} are practically insensitive to changes in the equatorial ligand, whereas those of C^2_{2p} show larger variations. Thus changes in total spin density and in λ^2 reflect primarily changes in values of C^2_{2p}. The two new complexes exhibit values for the latter quantities that are in the range observed for pyridine adducts of Ni(III) complexes with ligands derived from salicylaldehyde and aliphatic diamines, but no correlation with the bulkiness of the aliphatic imine bridge could be extracted from the data, probably due to the limited number of complexes studied.

4. Concluding remarks

The oxidation of [Ni(saldMe)] and [Ni(salhd)] in DMF and $(CH_3)_2SO$ (strong donor solvents) was shown to proceed through oxidation of the metal centre and with concomitant axial coordination of solvent molecules, as has been observed for [Ni(salen)] and [Ni(saltMe)], giving Ni(III) complexes formulated as $[Ni(L)(solv)_2]^+$, where L is a Schiff base and solv a solvent molecule.

X-ray structure of the complexes revealed that in [Ni(saltMe)] two methyl groups of the imine bridge are perpendicular to the equatorial plane and directed towards the two axial coordination positions, whereas in [Ni(saldMe)] only one methyl group is directed towards one axial position. It is to be expected also that in the *cis* isomer of [Ni(salhd)] the cyclohexane group is directed towards one of the axial positions. Thus the required axial coordination of solvent molecules in these electrogenerated Ni(III) species is hindered sterically when compared with [Ni(salen)] and the main result is that the sequence observed for the $E_{1/2}$ values, [Ni(salen)] < [Ni(salhd)] ≤ [Ni(saldMe)] < [Ni(saltMe)], parallels the hindrance on axial coordination. Thus, bulky substituents in the imine bridge tend to render less accessible the +3 oxidation state in Ni(II) complexes with the N_2O_2 Schiff base ligands.

Supplementary data

Crystallographic data (excluding structure factors) for the structures in this paper have been deposited with the Cambridge Crystallographic Data Centre as supplementary publications nos. CCDC 133149 {[Ni(saldMe)]} and CCDC 133150 {[Ni(saltMe)]}. Copies of the data can be obtained, free of charge, on application to CCDC, 12 Union Road, Cambridge CB2 1EZ, UK, (fax: +44-1223-336033 or e-mail: deposit@ccdc.cam.ac.uk).

Acknowledgements

This work was partially supported by the 'Fundação para a Ciência e Tecnologia' (F.C.T.) through project PBIC/QUI/2137/95. M.V.-B. thanks the FCT/Praxis XXI for a fellowship.

References

[1] C. Gosden, K.P. Healy, D. Pletcher, J. Chem. Soc., Dalton Trans. (1978) 972.
[2] K.P. Healy, D. Pletcher, J. Organomet. Chem. 186 (1980) 401.
[3] C. Gosden, J.B. Kerr, D. Pletcher, R. Rosas, J. Electroanal. Chem. Interfacial Electrochem. 117 (1981) 101.
[4] C.E. Dahm, D.G. Peters, J. Electroanal. Chem. Interfacial Electrochem. 406 (1996) 119.
[5] B. Castro, C. Freire, Inorg. Chem. 29 (1990) 5113.
[6] M.A.A.F. de C.T. Carrondo, B. Castro, A.M. Coelho, D. Domingues, C. Freire, J. Morais, Inorg. Chim. Acta 205 (1993) 157.
[7] F. Azevedo, M.A.A.F. de C.T. Carrondo, B. Castro, M. Convery, D. Domingues, C. Freire, M.T. Duarte, K. Nielsen, I.C. Santos, Inorg. Chim. Acta 219 (1994) 43.
[8] C. Freire, B. Castro, J. Chem. Soc., Dalton Trans. (1998) 1491.
[9] C. Freire, B. Castro, Polyhedron 17 (1998) 4227.
[10] M. Vilas-Boas, C. Freire, B. Castro, A.R. Hillman, P.A. Christensen, Inorg. Chem. 36 (1997) 4929.
[11] M. Vilas-Boas, C. Freire, B. Castro, A.R. Hillman, J. Phys. Chem. B 102 (1998) 8533.
[12] K.A. Goldsby, J. Coord. Chem. 19 (1988) 83.
[13] K.A. Goldsby, L.A. Hoferkamp, Chem. Mater. 1 (1989) 348.
[14] P. Audebert, P. Capdevielle, M. Maumy, New J. Chem. 15 (1991) 235.
[15] P. Audebert, P. Capdevielle, M. Maumy, New J. Chem. 16 (1992) 697.
[16] R.H. Holm, G.W. Everett, A. Chakravorty, Prog. Inorg. Chem. 7 (1966) 183.
[17] G.M. Sheldrick, in: G.M. Sheldrick, C. Kurger, R. Goddard (Eds.), Crystallographic Computing 3, Oxford University Press, Oxford, 1985, p. 175.
[18] G.M. Sheldrick, A Computer Program for Refinement of Crystal Structures (SHELXL-97), University of Göttingen.
[19] M.N. Burnett, C.K. Johnson, ORTEP III: Oak Ridge Thermal Ellipsoid Plot Program for Crystal Structure Illustrations, Oak Ridge National Laboratory Report ORNL-6895, 1996.
[20] International Tables for X-Ray Crystallography, vol. IV, Kynoch Press, Birmingham, 1974.
[21] G. Maki, J. Chem. Phys. 28 (1958) 651.
[22] A. Wojtczak, E. Szlyk, M. Jaskólski, E. Larson, Acta Chem. Scand. 51 (1997) 274.
[23] A.G. Manfredotti, C. Guastini, Acta Crystallogr., Sect. C 39 (1983) 863.
[24] U. Casellato, P. Guerriero, S. Tamburini, P.A. Vigato, C. Benelli, Inorg. Chim. Acta 207 (1993) 39.
[25] A. Radha, M. Seshasayee, K. Ramalingam, G. Aravamudan, Acta Crystallogr., Sect. C 41 (1985) 1169.
[26] F. Akhtar, Acta Crystallogr., Sect. B 37 (1981) 84.
[27] M. Calligaris, G. Nardin, L. Randaccio, Coord. Chem. Rev. 7 (1972) 385.
[28] F.H. Allen, O. Kennard, R. Taylor, Acc. Chem. Res. 16 (1983) 146.
[29] F.H. Allen, J.E. Davies, J.J. Galloy, O. Johnson, O. Kennard, C.F. Macrae, G.F. Mitchell, G.F. Mitchell, J.M. Smith, D.G. Watson, J. Chem. Inf. Comput. Sci. 31 (1987) 187.
[30] A.J. Bard, L.R. Faulkner, Electrochemical Methods, Wiley, New York, 1980.
[31] A. Kapturkiewicz, B. Behr, Inorg. Chim. Acta 69 (1983) 247.
[32] B. Castro, C. Freire, E. Pereira, J. Chem. Soc., Dalton Trans. (1994) 571.
[33] B.R. McGarvey, Can. J. Chem. 53 (1975) 2498.
[34] G. Labause, J.B. Raynor, J. Chem. Soc., Dalton Trans. (1980) 2388.
[35] G. Labause, J.B. Raynor, J. Chem. Soc., Dalton Trans. (1981) 590.
[36] A.H. Maki, N. Edelstein, A. Davison, R.H. Holm, J. Am. Chem. Soc. 86 (1964) 4580.
[37] B.A. Goodman, J.B. Raynor, Adv. Inorg. Chem. Radiochem. 13 (1970) 135.
[38] P. McArdle, J. Appl. Crystallogr. 28 (1995) 65.